Journal of Magnetic Resonance 202 (2010) 239–244

Contents lists available at ScienceDirect

Journal of Magnetic Resonance

journal homepage: www.elsevier.com/locate/jmr

Reduction of B_0 inhomogeneity effects in triple-quantum-filtered sodium imaging

Christian Matthies [a,*], Armin M. Nagel [a], Lothar R. Schad [b], Peter Bachert [a]

[a] Department of Medical Physics in Radiology, Deutsches Krebsforschungszentrum, Im Neuenheimer Feld 280, 69120 Heidelberg, Germany
[b] Computer Assisted Clinical Medicine, University of Heidelberg, Theodor-Kutzer-Ufer 1-3, 68167 Mannheim, Germany

ARTICLE INFO

Article history:
Received 23 October 2008
Revised 12 November 2009
Available online 18 November 2009

Keywords:
Sodium MRI
Multiple-quantum filter
Coherence
B_0 inhomogeneity

ABSTRACT

Triple-quantum (TQ) filtered sodium MR imaging has been proposed for separation of sodium signal arising from different physiological compartments. In a three-pulse sequence without refocussing pulse, the TQ signal is strongly sensitive to inhomogeneities of the B_0 field. We examine the dependence of the TQ signal intensity on the sequence parameters and propose a modified phase-cycling scheme to improve image quality. A new method for correction of B_0 inhomogeneity artefacts in TQ filtered sodium imaging is presented which requires only two acquisitions to obtain a correction as far as the B_0 inhomogeneity and the pulse widths are not too large. The method was verified in phantom experiments.

1. Introduction

Sodium (^{23}Na) plays a key role in many physiological processes and is thus a worthwile target of MRI, particularly since it yields the second strongest *in vivo* NMR signal [1–4]. Transmembrane sodium–potassium pumps generate a permanent gradient between the extracellular (Na^+_{ex}) and intracellular (Na^+_{in}) sodium concentration. A breakdown of this gradient indicates severe functional disorder in living tissue. An MR technique for selective imaging of intracellular sodium is therefore desirable.

Three methods for this purpose have been proposed so far. The first approach employs chemical-shift reagents that do not permeate the cell membranes to modify the resonance frequency of extracellular sodium [5,6]. These reagents are toxic, however, and cannot be applied to studies with humans. A second, non-invasive approach utilizes differences of relaxation rates in different physiological compartments for selective signal suppression via inversion recovery [7,8]. In this case, only one type of environment with one specific decay rate of the ^{23}Na transversal magnetization can be suppressed at once and regions with similar decay rates might be unintentionally suppressed.

The third and likewise non-invasive approach is to use a triple-quantum (TQ) filter selective for sodium ions that are restricted in their mobility. This restriction will occur because of interaction with macromolecular structures within the intracellular compartment [9–11]. Employing shift reagents, it has been shown in a rat liver study that most of the TQ filtered ^{23}Na signal originates from the intracellular compartment [12]. The problems arising with this method are low signal-to-noise ratio (SNR), strong dependence of the TQ signal intensity on the flip angle θ (with $\sin^5\theta$) and a pronounced sensitivity to B_0 inhomogeneities especially if a 180° refocussing pulse is omitted [13].

Hancu et al. showed that, compared to a four-pulse sequence including a 180° refocussing pulse, a three-pulse sequence has advantages for TQ filtered sodium imaging in humans due to less SAR and a B_1 dependence more amenable to subsequent corrections [11]. Yet, the lack of a refocussing pulse introduces a signal dependence on the B_0 inhomogeneity, since in that case relative phase shifts between the four coherence pathways contributing to the TQ signal are generated. Destructive interference then leads to a further loss of the already small signal.

Tanase and Boada suggested an algorithm to correct the TQ signal for B_0 inhomogeneities by acquiring four images and a B_0 map and solving a linear equation system for the four unknown signal components [13]. In the following, this method will be denoted by *method A*. Since the measurement of four images is time-consuming, we examined an alternative method (*method B*), which requires only two acquisitions to obtain a correction as far as the B_0 inhomogeneity and the pulse widths are not too large. First, the dependence of the TQ signal intensity on sequence parameters, particularly on the phase cycling angles, is studied, which, to our knowledge, has not been done so far. In a second step, from this information, the proposed method for B_0 inhomogeneity correction is deduced.

2. Theory

We consider a standard TQ coherence filtering sequence (Fig. 1). It consists of three radio frequency (RF) pulses with flip angle θ,

* Corresponding author.
E-mail address: c.matthies@dkfz.de (C. Matthies).

1090-7807/$ - see front matter © 2009 Elsevier Inc. All rights reserved.
doi:10.1016/j.jmr.2009.11.004

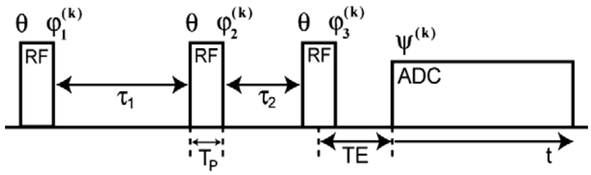

Fig. 1. Sequence employed for [23]Na TQ filtering experiments: three RF pulses with flip angle θ, phases $\varphi_i^{(k)}(i = 1,2,3)$ and width T_P. Delay times between pulses: preparation time τ_1 and evolution time τ_2, typically $\tau_2 \ll \tau_1$. Signal acquisition (duration: t) starts after echo time TE with receiver (ADC) phase set to $\psi^{(k)}$.

phases $\varphi_1^{(k)}, \varphi_2^{(k)}, \varphi_3^{(k)}$ (where k specifies the choice of the pulse phases in the k-th cycle) and delay times τ_1 and τ_2 for preparation and evolution of TQ coherences, respectively. $\psi^{(k)}$ is the relative phase of the receiver.

We are interested in the effect of static B_0 inhomogeneities on the signal intensity of this experiment. To quantify the inhomogeneity in a particular voxel, we use the frequency offset δ of the applied RF frequency ω from the Larmor frequency $\omega_0 = \gamma B_0$ in this voxel:

$$\delta = \omega - \omega_0 = \gamma(B - B_0). \tag{1}$$

The signal $S_\delta^{(k)}$, obtained from that voxel, is a superposition of the partial signals from different coherence pathways passed through in the course of the sequence:

$$S_\delta^{(k)}(t) = \left| \sum_{m_1=-1}^{1} \sum_{m_2=-3}^{3} S_{m_1,m_2}^{(k)}(t) \right|. \tag{2}$$

The first pulse creates coherences of the order $m_1 = -1$ and $m_1 = +1$ (besides possibly remaining longitudinal magnetization of order 0), which the second pulse converts into coherences between orders $m_2 = -3$ and up to $m_2 = +3$. The third pulse is applied to transform TQ coherence into detectable transverse magnetization. The altogether 21 possible coherence pathways are uniquely determined by m_1 and m_2, and each signal component

$$S_{m_1,m_2}^{(k)}(t) = A_{m_1,m_2}(t)\Phi_{m_1,m_2}^{(k)}\Delta_{m_1,m_2} \tag{3}$$

is the product of an amplitude A_{m_1,m_2} depending on the flip angle and the delay times, a phase factor

$$\Phi_{m_1,m_2}^{(k)}\left(\varphi_1^{(k)}, \varphi_2^{(k)}, \varphi_3^{(k)}, \psi^{(k)}\right) = e^{i(m_1\varphi_1^{(k)} + (m_2-m_1)\varphi_2^{(k)} + (1-m_2)\varphi_3^{(k)} + \psi^{(k)})} \tag{4}$$

depending on the pulse phases and the receiver phase, and a second phase factor

$$\Delta_{m_1,m_2}(t;\tau_1,\tau_2,\delta) = e^{i(m_1\tau_1 + m_2\tau_2 + t)\delta} \tag{5}$$

originating from the B_0 inhomogeneity. Here, we took into account that for a given phase ϕ a coherence of order m accumulates an overall phase $m\phi$. Each of the three pulses with phases $\varphi_j^{(k)}$ transfers magnetization between coherence orders m_i and m_f which generates an additional phase of $(m_f - m_i)\varphi_j^{(k)}$.

The common TQ filter is realized by addition of the signals of N acquisitions

$$S_\delta^{TQ}(t) = \left| \sum_{k=0}^{N-1} S_\delta^{(k)}(t) \right| \tag{6}$$

with appropriate choice of pulse and receiver phases for each signal. A phase-cycling scheme frequently used [11,13] is

$$\begin{aligned} &\varphi_1^{(k)} = \alpha_1 + k\frac{\pi}{3}, \quad \varphi_2^{(k)} = \alpha_2 + k\frac{\pi}{3}, \quad \varphi_3^{(k)} = 0, \\ &\psi^{(k)} = k\pi, \quad k = 0,1,2,3,\ldots \end{aligned} \tag{7}$$

The two starting phases α_1 and α_2 of the cycle determine essentially the signal yield. If the number N of acquired signals is a multiple of 6, only signal components that result from TQ coherence add up constructively while all other signal components cancel. As a consequence, only four components ($m_1 = \pm1$, $m_2 = \pm3$) survive in the measured TQ signal:

$$S_\delta^{TQ} = \left| S_{-1,-3}^{TQ} + S_{-1,+3}^{TQ} + S_{+1,-3}^{TQ} + S_{+1,+3}^{TQ} \right|. \tag{8}$$

Each of these components of the TQ filtered signal

$$S_{m_1,m_2}^{TQ}(t) = A_{m_1,m_2}(t)\overline{\Phi}_{m_1,m_2}\Delta_{m_1,m_2} \quad (m_1 = \pm1, m_2 = \pm3) \tag{9}$$

looks similar to Eq. (3), except for the pulse phase factor (denoted by $\overline{\Phi}$), which now merely depends on the starting phases of the cycle:

$$\overline{\Phi}_{m_1,m_2} = 6e^{i(m_1\alpha_1 + (m_2-m_1)\alpha_2)}. \tag{10}$$

The amplitudes A_{m_1,m_2} for $m_1 = \pm1$ and $m_2 = \pm3$

$$A_{m_1,m_2}(t) = F(t;\tau_1,\tau_2)D_{m_1,m_2}(\theta) \tag{11}$$

are composed (up to a normalization factor) of a factor

$$F(t;\tau_1,\tau_2) = f_{31}^1(\tau_1)f_{33}^3(\tau_2)f_{31}^1(t) \tag{12}$$

that accounts for relaxation during preparation and evolution of the TQ coherences and that is independent of the pathway characterized by m_1 and m_2. The relaxation of a spin-3/2 nucleus is biexponential, i.e.

$$f_{31}^1(t) \propto e^{-t/T_{2S}} - e^{-t/T_{2L}} \quad \text{and} \quad f_{33}^3(t) \propto e^{-t/T_{2L}}, \tag{13}$$

in the case of sufficiently long correlation times ($\tau_c > 1/\omega_0$) of the ion tumbling motion [9]. The other factor in Eq. (11)

$$D_{m_1,m_2}(\theta) = d_{m_1 0}^1(\theta)d_{m_2 m_1}^3(\theta)d_{1 m_2}^1(\theta) \tag{14}$$

depends on the flip angle θ. The transfer of magnetization between coherence orders m_i and m_f for each pulse is weighted by Wigner d-matrix elements $d_{m_f m_i}^r(\theta)$, where r is the rank of the magnetization tensor at the time of the particular pulse. For the signal components passing the TQ filter we finally obtain

$$\begin{pmatrix} D_{-1,-3}(\theta) \\ D_{-1,+3}(\theta) \\ D_{+1,-3}(\theta) \\ D_{+1,+3}(\theta) \end{pmatrix} = \sin^5(\theta) \begin{pmatrix} \cos^2(\theta/2)\sin^2(\theta/2) \\ \cos^2(\theta/2)\sin^2(\theta/2) \\ -\sin^4(\theta/2) \\ -\cos^4(\theta/2) \end{pmatrix}. \tag{15}$$

Further analysis of multiple quantum coherence for spin-3/2 nuclei can be found in [13–15].

3. Material and methods

Experiments were carried out on a clinical 3-T whole-body MR tomograph (Magnetom Trio; Siemens Medical Solutions, Erlangen, Germany). Excitation and signal detection were performed with a double-resonant (32.6 MHz/123.2 MHz) birdcage coil (Rapid Biomed GmbH, Würzburg, Germany). For MRI the TQ filtering sequence (Fig. 1) was combined with a density-adapted 3D radial acquisition scheme [16]. Image reconstruction was performed offline with Matlab (Mathworks, Natick, MA, USA). A Kaiser–Bessel gridding kernel with an oversampling ratio of two and additional Hanning filtering were applied.

We used a phantom consisting of a 500 ml plastic bottle filled with 2.5% agarose gel and 1 mol/l sodium chloride. Agarose gel was employed to constrain the tumbling motion of the sodium ions which is a prerequisite for creation of TQ coherences. Before measurement, the standard shim procedure provided by the manufacturer was applied.

Two single-quantum sodium images with different echo times TE_1 and TE_2 were acquired yielding phase maps Φ_1 and Φ_2 from which the inhomogeneity parameter

$$\delta = \frac{\Phi_2 - \Phi_1}{TE_2 - TE_1} \tag{16}$$

was calculated for each voxel within the phantom [13].

TQ filtered sodium images were acquired with echo time $TE = 8$ ms, preparation time $\tau_1 = 8$ ms and evolution time $\tau_2 = 50$ µs. The repetition time ($TR = 85$ ms) and the pulse width ($T_P = 0.5$ ms) were chosen to obey the SAR limits. 2000 projections and 6 mm isotropic resolution yielded a field of view of 150 mm. The acquisition time was 15 min. For B_0 inhomogeneity correction with *method A*, starting phases α_1/α_2 were set to 30°/120°, 120°/120°, 45°/90°, and 60°/75° [13], $N = 6$ averages were taken. For *method B*, starting phases α_1/α_2 were chosen as 30°/120° and 120°/120°, and again $N = 6$ averages were taken. In addition, images with $\alpha_1/\alpha_2 = 30^\circ/150^\circ$ and 120°/150° were acquired.

To compare *method A* with *method B*, also images with $\alpha_1/\alpha_2 = 30^\circ/120^\circ$ and 120°/120° and $N = 12$ averages were obtained, so that the same acquisition time could be employed for both methods. SNR calculations were performed afterwards by estimating the noise from difference images [17].

4. Results

In the following, we take $\theta = 90^\circ$ and calculate from Eq. (8), using Eqs. (9)–(11),

$$S_\delta^{\mathrm{TQ}}(t;\alpha_1,\alpha_2,\tau_1,\tau_2) = 24F(t;\tau_1,\tau_2)|\sin(\alpha_1 - \alpha_2 + \delta\tau_1) \times \cos(3\alpha_2 + 3\delta\tau_2)|, \tag{17}$$

where the global phase factor $e^{i\delta t}$ was omitted. Eq. (17) yields the symmetry relations

$$S_\delta^{\mathrm{TQ}}(t;\alpha_1 + (p + n/3)\pi, \alpha_2 + n\pi/3, \tau_1, \tau_2) = S_\delta^{\mathrm{TQ}}(t;\alpha_1,\alpha_2,\tau_1,\tau_2), \tag{18}$$

where $n, p = 0, \pm 1, \pm 2, \ldots$. Consequently, the combination $\alpha_1/\alpha_2 = 0^\circ/0^\circ$, employed in [13], is equivalent to $\alpha_1/\alpha_2 = 120^\circ/120^\circ$.

Taking relaxation into account, the preparation time τ_1 must be chosen close to

$$\tau_1^{(\mathrm{opt})} = \frac{T_{2L}T_{2S}}{T_{2L} - T_{2S}} \ln \frac{T_{2L}}{T_{2S}} \tag{19}$$

to maximize $f_{31}^1(\tau_1)$ [9], while τ_2 must be kept as short as possible to maximize $f_{33}^3(\tau_2)$ (Eqs. (12) and (13)). Usually, these requirements yield the condition

$$\tau_2 \ll \tau_1. \tag{20}$$

Accordingly, in S_δ^{TQ} (Eq. (17)) we have one δ-dependent sine factor rapidly oscillating (with τ_1) which is modulated at a much lower frequency (with τ_2) given by the cosine factor. We will call the former *oscillation factor* and the latter *modulation factor*.

Fig. 2 shows plots of S_δ^{TQ} as a function of the B_0 inhomogeneity δ for different combinations of α_1/α_2 and τ_1/τ_2. Extinctions in TQ signal intensity due to destructive interference of the four signal components for particular combinations of the measurement parameters are clearly visible.

The parameters for maximal signal intensity can be determined via the TQ signal dependence on α_1, α_2, τ_1, τ_2, and δ (Eq. (17)). Taking relaxation into account, τ_1 and τ_2 should be chosen as discussed in the context of Eq. (19). The parameter δ is mainly fixed by the quality of the shim, hence, only the adjustment of α_1 and α_2 is usable for optimization of the TQ signal intensity.

We obtain intensity minima from the oscillation factor if δ equals

$$\delta_{\min} = \frac{n\pi - (\alpha_1 - \alpha_2)}{\tau_1} \tag{21}$$

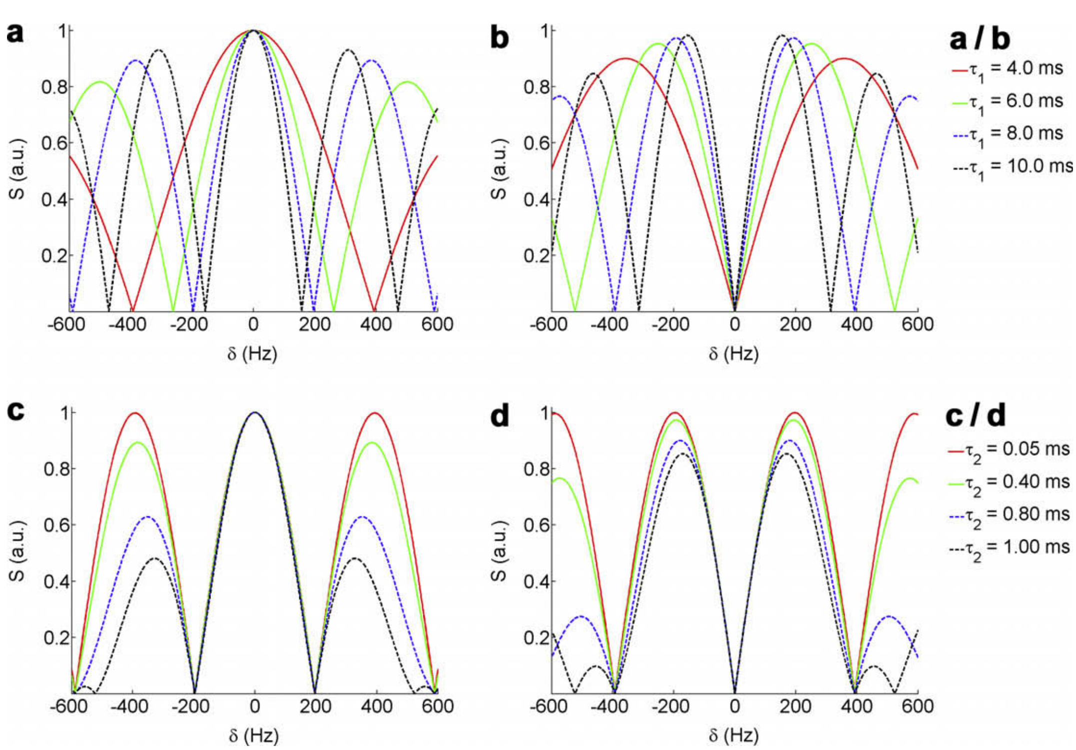

Fig. 2. TQ signal intensity S_δ^{TQ} as a function of δ for different values of τ_1/τ_2 and different combinations of α_1/α_2, setting $F(t;\tau_1,\tau_2) = 1/24$ for normalization. (a) $\alpha_1/\alpha_2 = 30^\circ/120^\circ$, $\tau_2 = 400$ µs; (b) $\alpha_1/\alpha_2 = 120^\circ/120^\circ$, $\tau_2 = 400$ µs; (c) $\alpha_1/\alpha_2 = 30^\circ/120^\circ$, $\tau_1 = 8$ ms; (d) $\alpha_1/\alpha_2 = 120^\circ/120^\circ$, $\tau_1 = 8$ ms.

and intensity minima from the modulation factor if δ equals

$$\delta_{\min}^{(\mathrm{mod})} = \frac{(2n+1)\pi/6 - \alpha_2}{\tau_2}, \tag{22}$$

where $n = 0, \pm 1, \pm 2, \ldots$. For $\tau_2 \ll 1/\delta$ the δ-dependence introduced by the modulation factor can be neglected and intensity minima only arise due to the oscillation factor. For larger values of τ_2 the influence of the modulation factor on the overall dependence of the TQ signal intensity on the B_0 inhomogeneity increases and additional intensity minima due to the modulation factor arise (Fig. 2c and d for $\tau_2 = 1$ ms). If we neglect the δ-dependence of the TQ signal due to the modulation factor, which is justified, regarding Eq. (20), for $\alpha_1/\alpha_2 = 30^\circ/120^\circ$, Eq. (21) reduces to $\delta_{\min} = \pm\frac{\pi}{2\tau_1}$ for the first minima of the signal intensity adjacent to the central maximum. With typical values for τ_1 in the range of 4–8 ms this results in signal intensity minima at frequency offsets of around 200–400 Hz (Fig. 2a). But even if the frequency offsets are lower, there may still be strong TQ signal reduction. Taking into account that 1 ppm — a typical order of B_0 inhomogeneity — corresponds to 33.8 Hz ($B_0 = 3$T) and 78.9 Hz ($B_0 = 7$T), respectively, extinction artefacts due to B_0 inhomogeneity are an issue to be considered especially for field strengths beyond 3 T.

Obviously, the combination $\alpha_1/\alpha_2 = 30^\circ/120^\circ$ — commonly employed — is a good choice if the field is highly homogeneous or if at least the preparation time τ_1 can be chosen sufficiently small (Fig. 2a).

The combination $\alpha_1/\alpha_2 = 120^\circ/120^\circ$ (Fig. 2b), which is complementary to 30°/120° (see below), is unfavorable if the B_0 field is exceptionally homogeneous or if τ_1 can be chosen small. However, in other cases, especially for frequency offsets in the range of 100–300 Hz (depending on τ_1) this combination would be preferable compared to 30°/120° (Fig. 2b).

Eq. (21) suggests two possible methods to control (via τ_1, or α_1 and α_2) the position of the signal intensity minima and maxima to obtain favorable measuring conditions with respect to given B_0 inhomogeneity in the MR system. Smaller τ_1 are preferable, because the maxima become broader (Fig. 2a/b), hence the signal dependence on δ is weaker. However, the decrease of τ_1 is limited by the condition to maximize $F(t; \tau_1, \tau_2)$ (Eq. (13)). Therefore, the better approach is to select appropriate values for α_1 and α_2 which can be done without restriction.

Optimization of the TQ signal for a given B_0 inhomogeneity can be performed as follows: First, the modulation factor has to be considered as it determines the expected maximum signal intensity. Maxima occur for values of α_2 of

$$\alpha_2^{(\mathrm{opt})} = \frac{n\pi}{3} - \delta\tau_2, \quad n = 0, \pm 1, \pm 2, \ldots \tag{23}$$

If the evolution time τ_2 is short enough compared to $1/\delta$, which should normally be the case, this reduces to $\alpha_2^{(\mathrm{opt})} = n\pi/3$. Only if the B_0 inhomogeneity is too large (in comparison to $1/\tau_2$), different values for α_2 might be optimal for different regions of the measured object. In the next step, variation of α_1 enables fine-tuning of the position of the maximum signal intensity with respect to the given inhomogeneity δ.

So far, the problem caused by the destructive influence of B_0 inhomogeneities on the TQ signal intensity is tackled indirectly. Eq. (17) suggests a method to remove the effect directly: First, a *complementary* TQ signal $\widetilde{S}_\delta^{\mathrm{TQ}}$ with

$$\begin{aligned}\widetilde{S}_\delta^{\mathrm{TQ}} &= S_\delta^{\mathrm{TQ}}(\alpha_1 + (2n+1)\pi/2, \alpha_2, \tau_1, \tau_2)\\ &= 24F(t; \tau_1, \tau_2)|\cos(\alpha_1 - \alpha_2 + \delta\tau_1)\cos(3\alpha_2 + 3\delta\tau_2)|,\\ &\quad (n = 0, \pm 1, \pm 2, \ldots)\end{aligned} \tag{24}$$

is acquired, leading to a phase shift of the oscillation factor by $\pi/2$. In the corrected signal

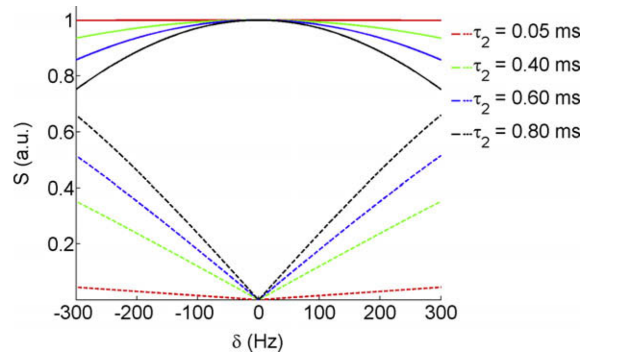

Fig. 3. Signal intensities of the corrected signals $S_{\mathrm{corr1}}^{\mathrm{TQ}}$ (Eq. (25), solid lines) and $S_{\mathrm{corr2}}^{\mathrm{TQ}}$ (Eq. (27), dashed lines) as a function of B_0 inhomogeneity δ for different values of $\tau_2 (\tau_1 = 8\ \mathrm{ms}, \alpha_2 = 120^\circ)$ and setting $F(t; \tau_1, \tau_2) = 1/24$ for normalization.

$$S_{\mathrm{corr1}}^{\mathrm{TQ}} = \sqrt{\left(S_\delta^{\mathrm{TQ}}\right)^2 + \left(\widetilde{S}_\delta^{\mathrm{TQ}}\right)^2} = 24F(t; \tau_1, \tau_2)|\cos(3\alpha_2 + 3\delta\tau_2)| \tag{25}$$

the oscillation factor has disappeared. The residual δ-dependence is much weaker (Fig. 3) and vanishes for $\tau_2 \ll 1/(3\delta)$.

Using a whole-body MR scanner, due to hardware and SAR limits, the pulse width T_P cannot be made arbitrarily short. The consequence is dephasing during application of the RF pulses which can be taken into account by addition of an effective time $T^{(\mathrm{eff})} = 2T_P/\pi$ (for $\theta = 90^\circ$) to the preparation and evolution time [13]. For $T_P = 500\ \mu$s, $T^{(\mathrm{eff})}$ amounts to 318 μs. This has a small influence on the preparation time τ_1, but a strong effect on the evolution time τ_2 (which might be even shorter than $T^{(\mathrm{eff})}$) and thus also on the dependence of the corrected signal on δ (Eq. (25)).

For a complete removal of the TQ signal dependence on δ, it is necessary to get also rid of the modulation factor in Eq. (25). This is achieved by the acquisition of two additional signals

$$\begin{aligned}S_\delta'^{\mathrm{TQ}} &= S_\delta^{\mathrm{TQ}}(\alpha_1', \alpha_2 + (2n+1)\pi/6, \tau_1, \tau_2),\\ \widetilde{S}_\delta'^{\mathrm{TQ}} &= S_\delta^{\mathrm{TQ}}(\alpha_1' + (2p+1)\pi/2, \alpha_2 + (2n+1)\pi/6, \tau_1, \tau_2),\\ &\quad (n, p = 0, \pm 1, \pm 2, \ldots)\end{aligned} \tag{26}$$

which define a second corrected signal

$$\begin{aligned}S_{\mathrm{corr2}}^{\mathrm{TQ}} &= \sqrt{\left(S_\delta'^{\mathrm{TQ}}\right)^2 + \left(\widetilde{S}_\delta'^{\mathrm{TQ}}\right)^2}\\ &= 24F(t; \tau_1, \tau_2)|\sin(3\alpha_2 + 3\delta\tau_2)|.\end{aligned} \tag{27}$$

Combining Eqs. (25) and (27) gives,

$$S_{\mathrm{corr3}}^{\mathrm{TQ}} = \sqrt{\left(S_{\mathrm{corr1}}^{\mathrm{TQ}}\right)^2 + \left(S_{\mathrm{corr2}}^{\mathrm{TQ}}\right)^2} = 24F(t; \tau_1, \tau_2), \tag{28}$$

which is independent of δ and thus of the inhomogeneities in the B_0 field. Fig. 3 shows plots of the expected signal intensities of the corrected signals $S_{\mathrm{corr1}}^{\mathrm{TQ}}$ (Eq. (25)) and $S_{\mathrm{corr2}}^{\mathrm{TQ}}$ (Eq. (27)) as a function of δ for different values of τ_2. Compared to the non-corrected TQ signals (Fig. 2), their dependence on δ is significantly reduced.

Fig. 4 shows results from measurements of the phantom. We chose a slice in which the effect of B_0 inhomogeneity was evident. Signal extinctions in the TQ filtered images (Fig. 4a, b, f, and g) are clearly visible. According to the corresponding phase map (Fig. 4k), the frequency offset in the central regions of the phantom amounts to up to 140 Hz, and the TQ signal with $\alpha_1/\alpha_2 = 30^\circ/120^\circ$ — as predicted by theory (Fig. 2a, $\tau_1 = 8$ ms) — is diminished there (Fig. 4a). The complementary TQ experiment with $\alpha_1/\alpha_2 = 120^\circ/120^\circ$ (Fig. 2b, $\tau_1 = 8$ ms) provides the signal missing in the first image (Fig. 4b) such that the combination of both TQ filtered images (Figs. 4a and b) calculated according to Eq. (25) yields a good correction for the signal extinctions due to B_0 inhomogeneity (Fig. 4c).

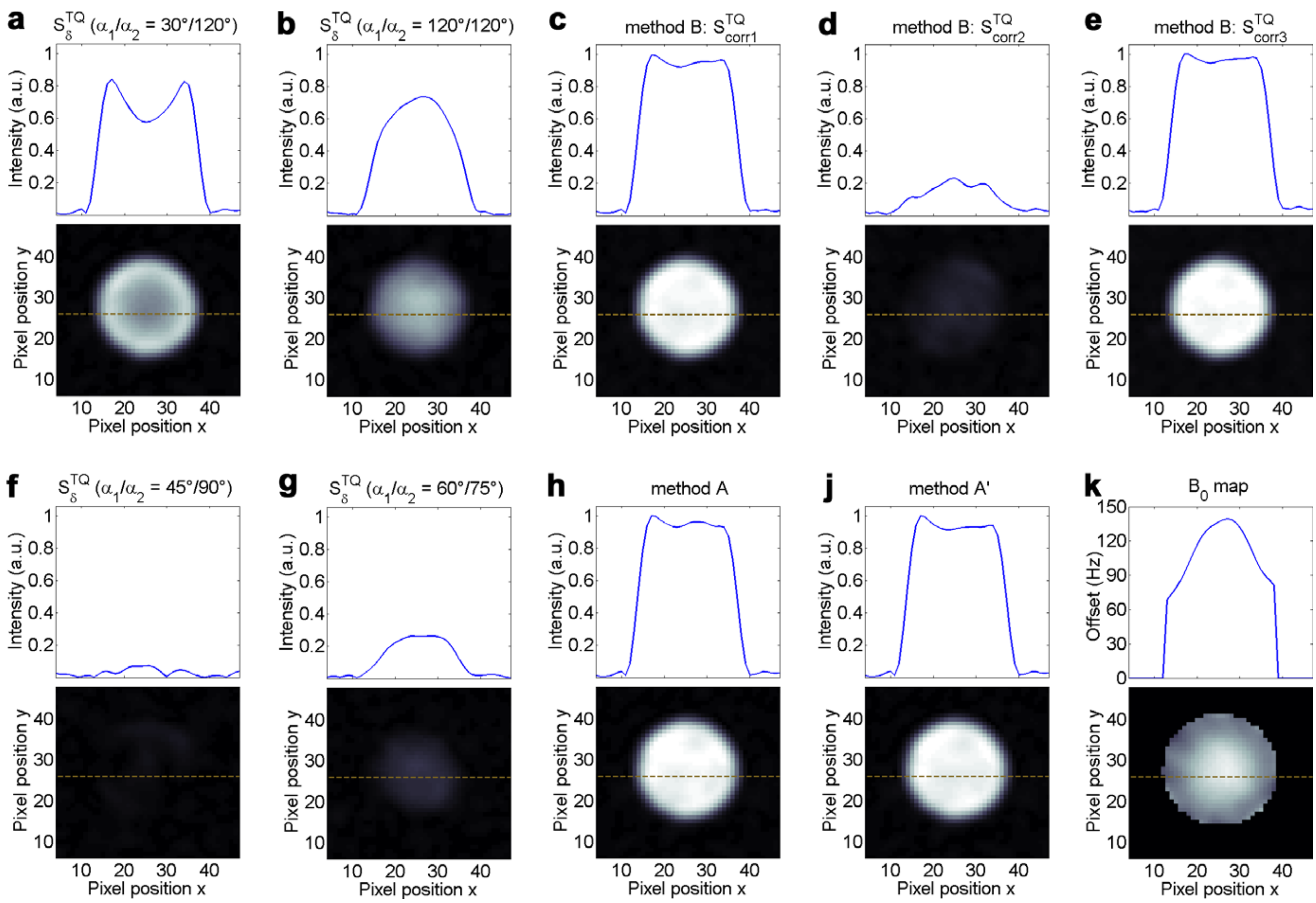

Fig. 4. Experimentally acquired TQ filtered sodium MR images from a selected slice of the phantom, 1D profiles in the upper part of the plots are along the dashed line. Grayscale colormap in images (a)–(j) is black for zero signal and white for signal magnitude 1. Images (e), (h) and (j) were normalized to 1, images (a)–(d) and (f)–(g) were normalized to image (e). (a, b, f, and g) TQ magnitude images acquired with starting phases α_1/α_2 as indicated, (c) corrected TQ magnitude image calculated with data from (a) and (b) and use of Eq. (25), (d) corrected TQ magnitude image calculated with use of Eq. (27), (e) corrected TQ magnitude image calculated with data from (c) and (d) and Eq. (28), (h) TQ magnitude image corrected according to *method A* with data from (a)/(b)/(f)/(g), (j) TQ magnitude image corrected according to *method A'* with data from (a) and (b) and two zero images, (k) B_0 map calculated using Eq. (16).

This is confirmed by comparison with Fig. 4d which shows the second corrected signal S_{corr2}^{TQ} calculated from images with starting phases $\alpha_1/\alpha_2 = 30^\circ/150^\circ$ and $120^\circ/150^\circ$ and use of Eq. (27). It yields almost no further contribution to the fully corrected signal S_{corr3}^{TQ} (Fig. 4e, calculated with Eq. (28) and data from Fig. 4c and d) so that the difference between the correction from two acquired images (Fig. 4c) and the correction from four acquired images (Fig. 4e) is negligibly small for the given inhomogeneity. This agrees well with the results in Fig. 3.

The result of the B_0 inhomogeneity correction performed with *method A* is displayed in Fig. 4h. The four TQ source images obtained with starting phases according to [13] are shown in Fig. 4a, b, f, and g. With the given inhomogeneity in the particular slice, two of the images (Fig. 4f and g) yield almost no contribution to the corrected image since here the value of α_2 is not optimal regarding Eq. (23). In fact, it is possible to perform *method A* with only two acquired images and two zero images (denoted as *method A'*) but the acquired images must be complementary in the sense discussed in the context of Eq. (24). An example is shown in Fig. 4j with data from Fig. 4a and b.

Altogether, we observed that (with the employed parameters) *method B* yielded the same SNR compared to *method A'*, but 10–40% more SNR compared to *method A*, depending on the B_0 inhomogeneity.

5. Discussion

Multiple-quantum filtered sodium MRI without application of a refocussing pulse is sensitive to inhomogeneities in the B_0 field due to destructive interference between the partial signals from different coherence pathways. A simple solution would be to filter out only one of the four coherence pathways leading to TQ coherence, however, this would strongly reduce SNR. Otherwise, depending on the extent of B_0 inhomogeneity, the interference between the partial signals has to be taken into account.

Method A [13] requires the acquisition of four TQ images together with a B_0 map to obtain the inhomogeneity parameter δ for each voxel. The accuracy of the reconstructed image crucially depends on the exact knowledge of δ. Not all four required TQ images can be obtained with the same starting phase α_2 at the same time. In this case, the four signal equations would no longer be linearly independent so that the equation system could not be solved anymore. As a consequence, in the case of small B_0 inhomogeneity (compared to $1/\tau_2$) where all regions of interest exhibit almost the same $\alpha_2^{(opt)}$ (Eq. (23)), images with suboptimal signal intensity are acquired. In the worst case, only two of the four TQ images significantly contribute to the corrected image and the acquisition of the other two images can be abandoned (*method A'*).

In contrast, *method B*, usually requires only two TQ images. This advantage has to be traded off for the fact that the corrected signal in this method represents an estimate for the theoretically achievable signal. The goodness of the estimate, considering Eqs. (25) and (28), can be quantified by

$$\chi = S^{TQ}_{corr1} \Big/ S^{TQ}_{corr3} = |\cos(3\alpha_2 + 3\delta\tau_2)|, \tag{29}$$

which reduces to $\chi = |\cos(3\delta\tau_2)|$ in the case of $\alpha_2 = 120^\circ$. The smaller the B_0 inhomogeneity δ and evolution time τ_2 are the better the reconstruction of the theoretically achievable signal is. Fig. 3 shows that in our case ($T_P = 0.5$ ms, $\tau_2^{(eff)} = 0.4$ ms, δ up to 140 Hz), S^{TQ}_{corr1} is a very good estimate for $S^{TQ}_{corr3}(\chi = 0.998)$. Only if the condition $\delta\tau_2^{(eff)} \ll 1/3$ cannot be fulfilled, the acquisition of four TQ images will be necessary for the correction of B_0 inhomogeneities. This can occur if the inhomogeneity is large or if the pulse width T_P cannot be made short enough such that $\tau_2^{(eff)} \ll 1/(3\delta)$ is satisfied. Under these circumstances *method B* loses the advantage of a shorter overall acquisition time compared to *method A*. Otherwise, the twofold number of averages can be achieved within the same acquisition time and higher SNR is obtained. With *method B*, both images can be acquired with the optimal value for the starting phase α_2. No prior knowledge about the B_0 inhomogeneity in the system is required. Reversely, it is a kind of B_0 map that is obtained in this case. In contrast to *method A′*, *method B* provides an estimate for the accuracy of the correction (Eq. (29)).

We attribute the small intensity variations still present after correction for B_0 inhomogeneities mainly to Gibbs ringing artefacts, but intravoxel dephasing might also play a role.

In this work we put the focus on TQ filtered sodium imaging to selectively detect sodium ions restricted in motion. Yet, the suggested method for correction of B_0 inhomogeneities should perform equally well in investigations with double-quantum-filtered sodium imaging for detection of long-range order in biological systems. Regarding *in vivo* applications, lower sodium concentration requires larger voxel sizes or longer acquisition times, nevertheless, this should not have an effect on the applicability of the proposed method.

Presently, sodium MRI advances to high-field studies ($B_0 > 3$T). Then, the influence of B_0 inhomogeneities is even more critical and the proposed method for correction of such inhomogeneities could be particularly useful.

In conclusion, the quantitative dependence of the signal intensity in TQ filtered ^{23}Na MR imaging on measurement parameters as the starting phases α_1 and α_2 of the phase cycle and the B_0 inhomogeneity δ has been given. Techniques have been proposed to optimize the starting phases for maximum signal intensity before measurement thus reducing effects of B_0 inhomogeneity. The essence of a proposed method for correction of B_0 inhomogeneity artefacts is the reduction of the strong TQ signal dependence on δ with τ_1 and τ_2 to a much weaker δ-dependence with only τ_2 by acquiring a second, complementary TQ filtered image.

References

[1] R. Ouwerkerk et al., Tissue sodium concentration in human brain tumors as measured with ^{23}Na MR imaging, Radiology 227 (2003) 529–537.
[2] J.J. Sandstede et al., Time course of ^{23}Na signal intensity after myocardial infarction in humans, Magn. Reson. Med. 52 (2004) 545–551.
[3] F.E. Boada et al., Loss of cell ion homeostasis and cell viability in the brain: what sodium MRI can tell us, Curr. Top. Dev. Biol. 70 (2005) 77–101.
[4] S. Nielles-Vallespin et al., 3D radial projection technique with ultrashort echo times for sodium MRI: clinical applications in human brain and skeletal muscle, Magn. Res. Med. 57 (2007) 74–81.
[5] R.K. Gupta, P. Gupta, Direct observation of resolved resonances from intra- and extracellular sodium ions in NMR studies of intact cells and tissues using $Dy(PPP)_2^{7-}$, J. Magn. Res. 47 (1982) 344–350.
[6] N. Bansal et al., Thulium 1,4,7,10-tetraazacyclododecane-1,4,7,10-tetrakis (methylene phosphonate) as a ^{23}Na shift reagent for the in vivo rat liver, Biochemistry 32 (1993) 5638–5643.
[7] R. Stobbe, C. Beaulieu, In vivo sodium magnetic resonance imaging of the human brain using soft inversion recovery fluid attenuation, Magn. Res. Med. 54 (2005) 1305–1310.
[8] P. Rong, R.R. Regatte, A. Jerschow, Clean demarcation of cartilage tissue ^{23}Na by inversion recovery, J. Magn. Res. 193 (2008) 207–209.
[9] G. Jaccard, S. Wimperis, G. Bodenhausen, Multiple-quantum NMR spectroscopy of $S = 3/2$ spins in isotropic phase: a new probe for multiexponential relaxation, J. Chem. Phys. 85 (1986) 6282.
[10] R. Reddy, E.K. Insko, J.S. Leigh, Triple quantum sodium imaging of articular cartilage, Magn. Reson. Med. 38 (1997) 279–284.
[11] I. Hancu, F.E. Boada, G.X. Shen, Three-dimensional triple-quantum-filtered ^{23}Na imaging of in vivo human brain, Magn. Res. Med. 42 (1999) 1146–1154.
[12] V. Seshan, A.D. Sherry, N. Bansal, Evaluation of triple-quantum-filtered ^{23}Na NMR spectroscopy in the in situ rat liver, Magn. Res. Med. 38 (1997) 821–827.
[13] C. Tanase, F.E. Boada, Triple-quantum-filtered imaging of sodium in presence of B_0 inhomogeneities, J. Magn. Res. 174 (2005) 270–278.
[14] C. Tanase, F.E. Boada, Algebraic description of spin 3/2 dynamics in NMR experiments, J. Magn. Res. 173 (2005) 236–253.
[15] J.R.C. van der Maarel, Thermal relaxation and coherence dynamics of spin 3/2. I. Static and fluctuating quadrupoloar interactions in the multipole basis, Conc. Magn. Res. A 19 (2003) 97–116.
[16] A. Nagel et al., Sodium MRI using a density-adapted 3D radial acquisition technique, Mag. Reson. Med. 62 (2009), doi:10.1002/mrm.22157.
[17] National Electrical Manufacturers Association, Determination of Signal-to-Noise Ratio (SNR) in Diagnostic Magnetic Resonance Imaging, NEMA Standards Publication MS 1-2001, 2001.